SUPPLEMENTARY DATA

Measure and analysis of the DNA contour length from AFM images

Determination of the DNA contour length from digital images is not a trivial task. This is because during the digitization process, the exact contour of the DNA molecule is replaced by a discrete subset of pixels within a two dimensional grid. This approximation implies that the contour length of the original molecule can only be estimated rather than exactly measured and the reliability of such estimate will depend on both image resolution and the method employed to calculate the contour length from the chain of pixels. This further implies that although DNA molecules have the same number of bp, the binned contour length measurements result in a bell-shaped distribution that can be fitted with a Gaussian function to get the mean and the standard deviation. It has been shown that the contour length distribution of simulated DNA confined to a grid with sizes comparable to our AFM images, show a SD of about 8 nm (1). Surface interaction and instrumental noise can increase this value up to 50%. In the case of RNAP promoter complexes, the presence of a globular feature along the DNA path, as well as the possible presence of promoter complex intermediates having different conformations, can further increase the spread of the distribution. The presence of different intermediates may, in some cases, result in double- or multi-peak distributions that may not be fitted with a single Gaussian. For this reason, all the DNA contour length distributions reported in this study have been subjected to a normality test to justify fitting with a Gaussian function.

Determination of ppGpp-RNAP dissociation constant

Circular-dichroism spectroscopy (CD) was employed to determine the dissociation constant of ppGpp from RNAP. We titrated [ppGpp] from 0-100 μM keeping RNA polymerase concentration constant, and recorded the CD spectra in the range 210-250 nm for each ppGpp concentration (Fig. S1A). In agreement with previously reported data (2), the molar ellipticity of RNAP decreases as [ppGpp] increases, reaching a 19.7% decrease at 100 μM ppGpp. Fitting the 222 nm molar ellipticity at different [ppGpp] to the fractional saturation equation gives a K_d of 20.8 ±2.3 μM (Fig. S1B).

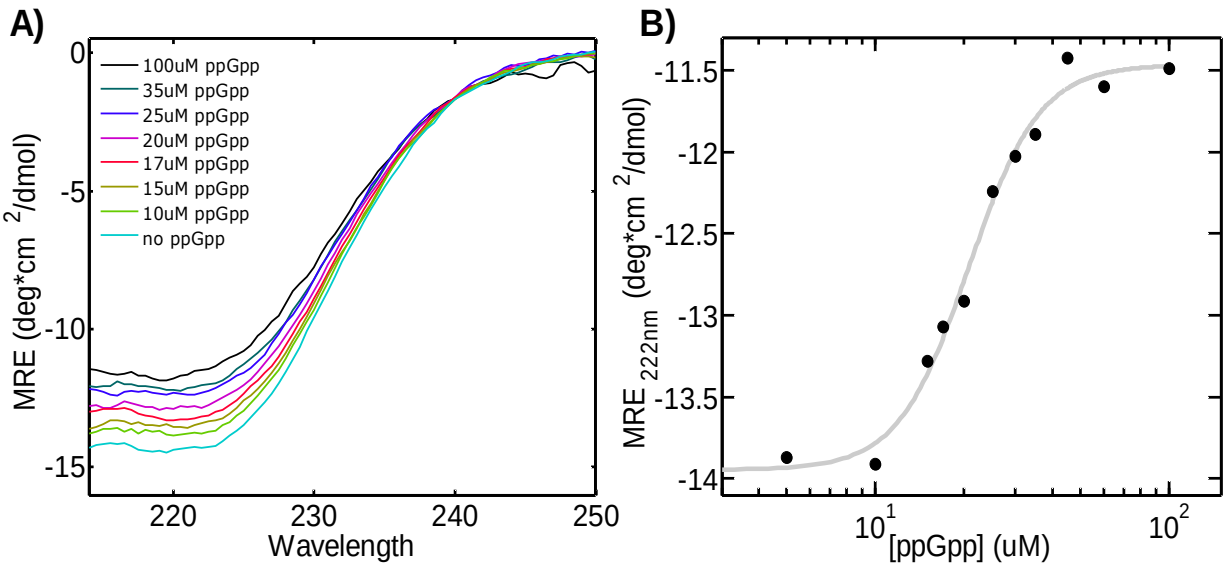

Supplementary Figure S1. A) Mean residue ellipticity (MRE) of RNAP at different [ppGpp], from 0 to 100 μM. Each color represents the CD spectra at each [ppGpp]. B) Mean residue ellipticity of RNAP at 222 nm at different [ppGpp]. The line represents the fitting the data points to the Hill equation.

Determination of the RNAP-promoter dissociation constants from AFM images

Determination of dissociation constants from AFM images of nucleoprotein complexes requires the assumption that the population of the different molecular species (free protein, free DNA and protein-DNA complexes) deposited on the surface are representative of those in solution. This means, in other words, that the deposition on the surface does not bias the population by selectively binding one or the other species. For instance, if the free DNA binds more efficiently onto mica than the proteinï DNA complexes, or if the mica favors dissociation of the nucleoprotein complexes, the apparent dissociation constant determined by AFM will be higher than the actual value. Conversely, if the proteinï DNA complexes deposit more efficiently than the free DNA, the apparent dissociation constant would be underestimated.

We have previously demonstrated that the transfer of DNA molecules from solution to the mica surface during sample preparation for AFM imaging is governed by diffusion and that the DNA molecules are irreversibly captured onto the surface by a network of magnesium ions linking the negatively charged DNA phosphates to the negative mica. Furthermore, within the first minutes of deposition, when the surface is not saturated by DNA molecules, the number of DNA fragments deposited is linear with time (3). Because under the condition used DNA fragments had one or two RNA polymerases bound, and because we did not

observe any increment of the number of DNA when RNAP was present, we conclude that the deposition of the complexes is driven by the DNA interaction with the mica surface. Regarding the stability of transcription complexes onto the surface we believe that under the deposition conditions used, mica does not disrupt transcription complexes because, in this and other study of these labs, we found a good correlation between promoter strength and promoter occupancy. In addition, the effects of the modulators ppGpp and DksA observed by AFM are in accordance with published data. Thus it is reasonable to conclude that AFM images of transcription complexes give a snapshot of the interaction governing the equilibrium of complex formation in solution, providing a powerful way for to the determination of binding constants and specificities. In order to determine the dissociation constants of promoter complexes assembled under different conditions we have employed a previously developed methodology which requires knowledge of the total RNAP and total DNA concentrations in the reaction, the fractional promoter occupancy and the average number of RNAP bound per DNA fragment. For clarity, below is reported the reverse of equation 5 in Yang 2005 (4) which we have used to determine the K_d.

$$K_d \approx \frac{(1 \text{ï } O_{SP}) \times ([P] \text{ï } [D] \times O_{Fragment})}{O_{SP}}$$

where: O_{SP} is the fractional promoter occupancy i.e. the ratio between the number of specific complexes and the total number of DNA molecules in the pool of images. $O_{Fragment}$ is the average number of RNAP bound per DNA which is obtained dividing the total number of complexes (specific and non-specific) by the total number of DNA molecules in the pool of images. [P] is the total RNAP concentration and [D] is the total DNA concentration. Note that the term ([P] ï [D] × $O_{Fragment}$) represents a better way to determine the free RNAP concentration. In fact, the total concentration of protein and the total concentration of DNA can readily be determined in the stock solutions, and because of the DNA driven deposition it is more reliable to count the DNA-bound RNAP than the free RNAP, for which the deposition process has not been thoroughly characterized. Note also that we could apply the approximated equation given in Yang 2005, because the DNA templates used in this work were linear, sufficiently long, contained a single promoter and the fractional occupancy was $<< 1$.

Because we did not know the DNA binding activity of the RNAP, we assumed that the RNAP stock solution was fully active. This assumption may lead to an overestimation of the K_d. For instance, if the RNAP would have been 50% active, the K_d will be one half of the value we

have determined. It must be pointed out, however, that the K_d values reported in this study are mainly used to compare RNAP binding affinities between experiments conducted in the presence and in the absence of modulators.

DksA purification

BL21 cells transformed with pET28(b) harboring the *dksA* gene were grown overnight at 37 °C in 1 liter of LB medium containing kanamycin. Cells were harvested and disrupted by sonication in Lysis Buffer (50 mM sodium phosphate pH 8.5, 300 mM NaCl, 10% glycerol, 1 mM ß-mercapto ethanol, 0.5 mM pepstatin, 1 mM leupeptin, 1 mM PMSF, 0.1% Tween-20 and 0.2 mg/ml lysozyme). The cell lysate supernatant was loaded onto a His-Trap FF column equilibrated with Buffer 1 (20 mM Tris-HCl pH 8.0, 250 mM NaCl, 20 mM imidazole) using an AKTA Prime system at 2 ml/min. The column was washed with five volumes of Buffer 1 followed by a 200 ml imidazole gradient from 0 to 500 mM; His6-DksA eluted at ~300 mM imidazole. Fractions containing the protein of interest were exchanged with Buffer 2 (20 mM Tris-HCl pH 8.0, 10 mM NaCl) and subjected to thrombin cleavage overnight at 25 °C. Completeness of the digestion was verified by SDS-PAGE (Fig. S7). The cleaved protein was loaded onto a disposable gravity column for ion-exchange chromatography equilibrated with the Buffer 2. The column was washed with ten volumes of the Buffer 3 (20 mM Tris-HCl pH 8.0, 20 mM NaCl). DksA was eluted with three column volumes of Buffer 4 (20 mM Tris-HCl pH 8.0, 500 mM NaCl). DksA was exchanged with storage buffer (20 mM Tris-HCl pH 8.0, 100 mM NaCl), and concentrated at 2 mg/ml by an Amicon System. The yield was 18 mg of purified protein per litre of culture broth. Protein was stored at -80 °C.

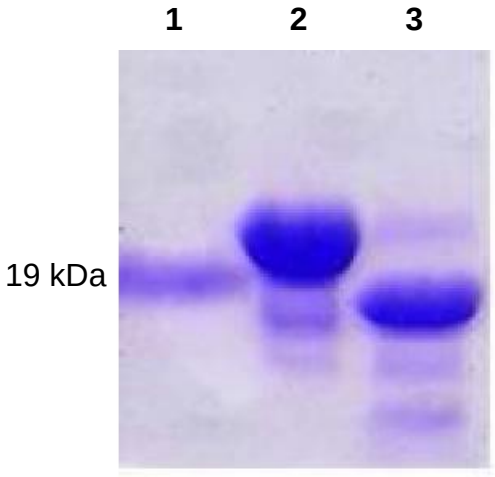

Supplementary Figure S2. SDS-PAGE analysis of the His-tag removal by thrombin cleavage. Lane 1) 19 kDa protein marker; lane 2) His6-tagged DksA (~20 kDa) after affinity chromatography; lane 3) thrombin cleaved DksA (~17.5 kDa). Gel was stained with Coomassie blue dye.

References

1. Rivetti, C. and Codeluppi, S. (2001) Accurate length determination of DNA molecules visualized by atomic force microscopy: evidence for a partial B- to A-form transition on mica. *Ultramicroscopy*, **87**, 55-66.

2. Woody, A.Y., Woody, R.W. and Malcolm, A.D. (1987) Effects of ppGpp on transcription by DNA-dependent RNA polymerase from Escherichia coli: circular dichroism, absorption and specific transcription studies. *Biochim Biophys Acta*, **909**, 115-125.

3. Rivetti, C., Guthold, M. and Bustamante, C. (1996) Scanning force microscopy of DNA deposited onto mica: equilibration versus kinetic trapping studied by statistical polymer chain analysis. *J Mol Biol*, **264**, 919-932.

4. Yang, Y., Sass, L.E., Du, C., Hsieh, P. and Erie, D.A. (2005) Determination of protein-DNA binding constants and specificities from statistical analyses of single molecules: MutS-DNA interactions. *Nucleic Acids Res*, **33**, 4322-4334.

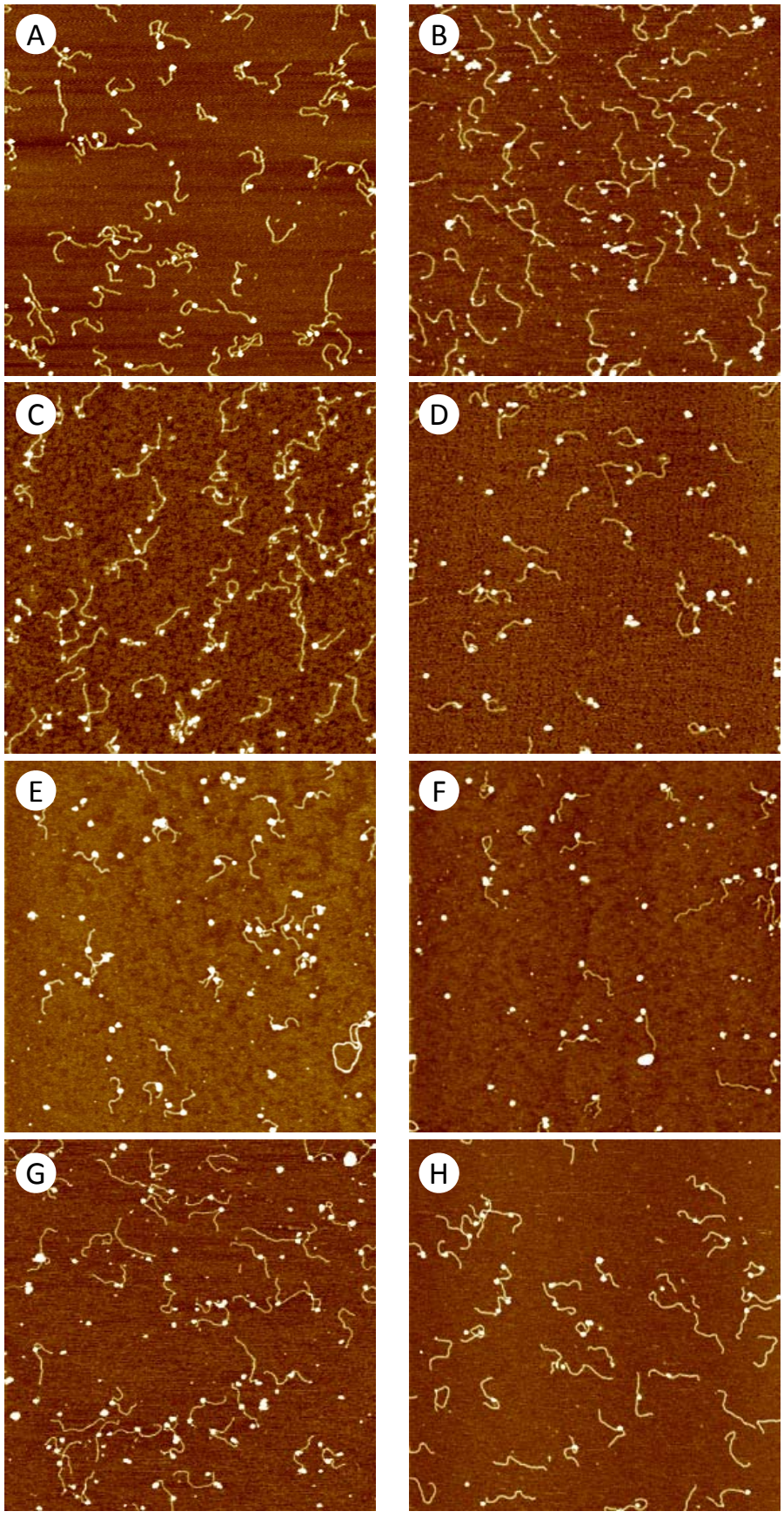

Supplementary Figure S3. Representative full-scan AFM images of promoter complexes under different conditions. A) *rrnB* P1 with no mdulators. B) *rrnB* P1 with 200 μM ppGpp and 650 nM DksA. C) *rrnA* P1 with no mdulators. D) *rrnA* P1 with 650 nM DksA. E) pR with no mdulators. F) pR with 200 μM ppGpp and 650 nM DksA. G) *rrnB* P1 (dis) with no mdulators. H) *rrnB* P1 (dis) with 200 μM ppGpp and 650 nM DksA. Scan size 2 μm.

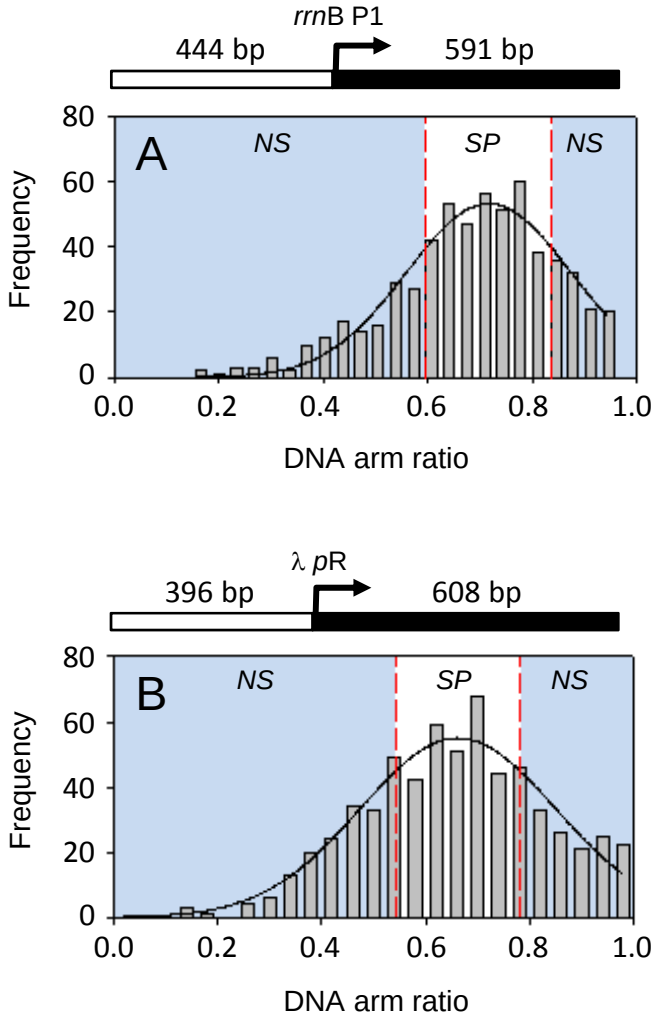

Supplementary Figure S4. Schematic representation of the arm ratio selection filter used to discriminate between specific (*SP*) and non-specific (*NS*) complexes. A) *rrnB* P1; B) λ pR.

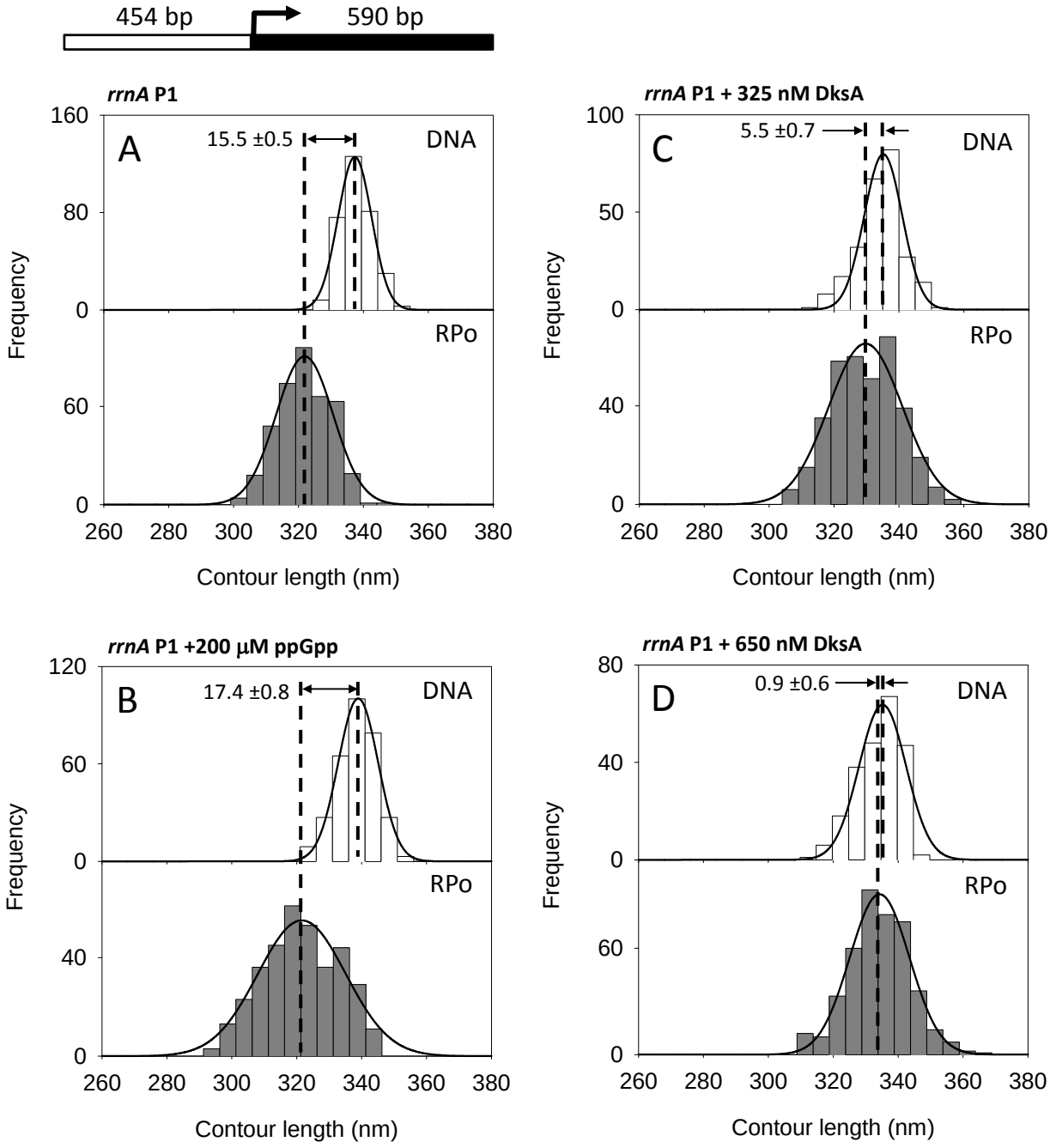

Supplementary Figure S5. DNA contour length distributions of bare DNA (top panel) and RPo (bottom panel) assembled onto a 1044 bp long DNA fragment harboring the *rrnA* P1 promoter near the center (top scheme). A) Without ppGpp. B) With 200 μM ppGpp. C) With 325 nM DksA. D) With 650 nM DksA.

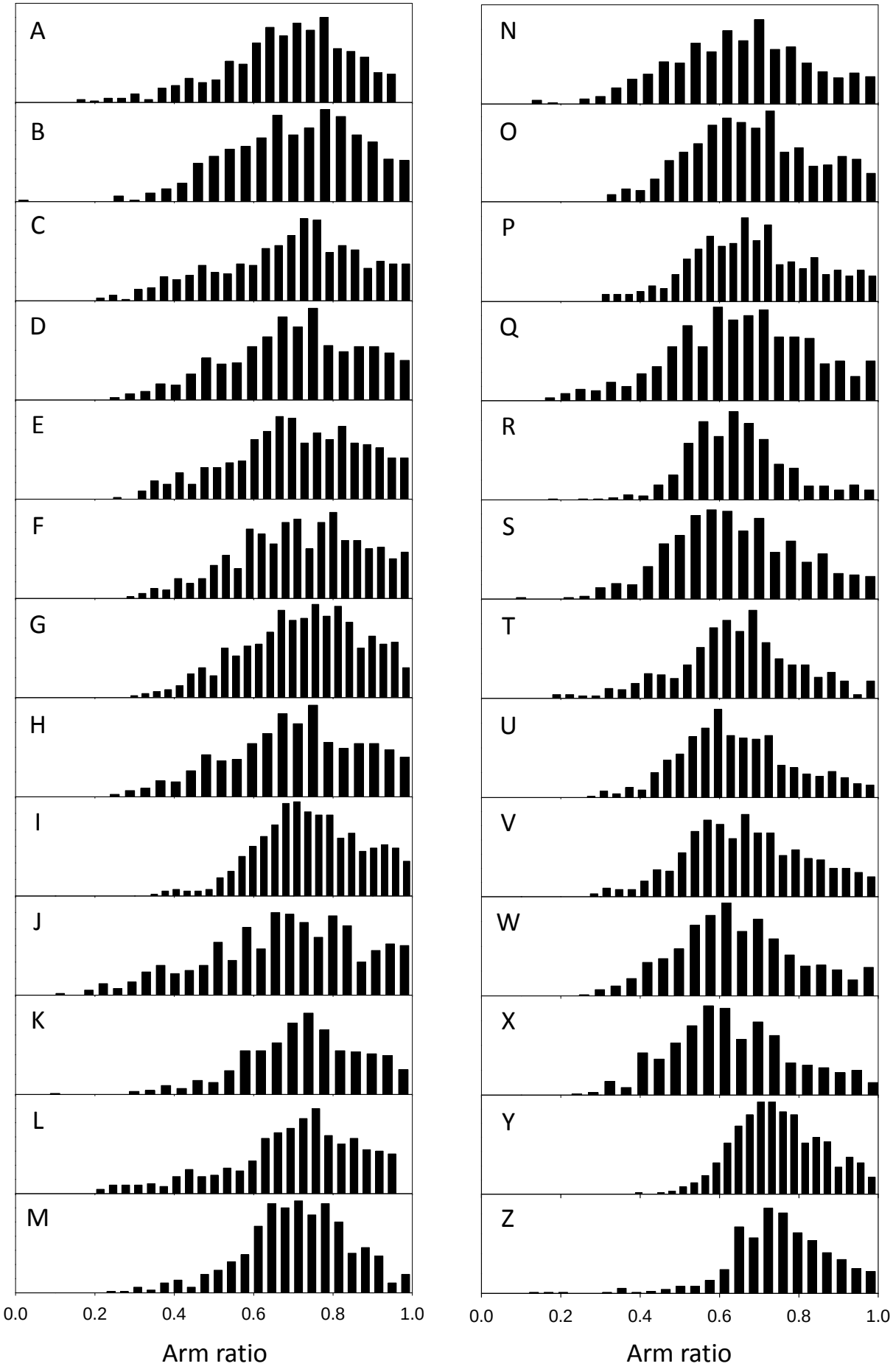
A
B
C
D
E
F
G
H
I
J
K
L
M
N
O
P
Q
R
S
T
U
V
W
X
Y
Z
0.0
0.2
0.4
0.6
0.8
1.0
Arm ratio
0.0
0.2
0.4
0.6
0.8
1.0
Arm ratio

Supplementary Figure S6. DNA arm ratio distributions obtained from the position of the RNAP relative to DNA ends for all the experiments reported in Table 1 (see last column for matching panels). (A-I) 1035 bp long DNA template harboring the *rrnB* P1 promoter. The expected value of the short arm/long arm ratio, relative to the TSS position, is 0.75. (J-M) 1044 bp long DNA template harboring the *rrnA* P1 promoter. The expected value of the short arm/long arm ratio, relative to the TSS position, is 0.77. (N-X) 1004 bp long DNA template harboring the pR promoter. The expected value of the short arm/long arm ratio, relative to the TSS position, is 0.65. (Y-Z) 1044 bp long DNA template harboring the mutant *rrnB* P1 (dis) promoter.